

Microscopic calculation of fission product yields with particle-number projectionMarc Verriere * and Nicolas Schunck*Nuclear and Chemical Sciences Division, Lawrence Livermore National Laboratory, Livermore, California 94551, USA*David Regnier *CEA, DAM, DIF, 91297 Arpajon, France**and Université Paris-Saclay, CEA, LMCE, 91680 Bruyères-le-Châtel, France*

(Received 19 January 2021; accepted 12 April 2021; published 3 May 2021)

Fission fragments' charge and mass distribution is an important input to applications ranging from basic science to energy production or nuclear nonproliferation. In simulations of nucleosynthesis or calculations of superheavy elements, these quantities must be computed from models, as they are needed in nuclei where no experimental information is available. Until now, standard techniques to estimate these distributions were not capable of accounting for fine-structure effects, such as the odd-even staggering of the charge distributions. In this work, we combine a fully microscopic collective model of fission dynamics with a recent extension of the particle number projection formalism to provide the highest-fidelity prediction of the primary fission fragment distributions for the neutron-induced fission of ^{235}U and ^{239}Pu . We show that particle-number projection is an essential ingredient to reproduce odd-even staggering in the charge yields and benchmark the performance of various empirical probability laws that could simulate its effect. This new approach also enables for the first time the realistic determination of two-dimensional isotopic yields within nuclear density functional theory.

DOI: [10.1103/PhysRevC.103.054602](https://doi.org/10.1103/PhysRevC.103.054602)**I. INTRODUCTION**

A predictive theory of nuclear fission has been a long-standing challenge of nuclear science that has gained renewed interest in recent years [1]. While fission is a fascinating problem on its own, as it involves the large-amplitude collective dynamics of a strongly interacting quantum many-body system, it also plays an important role in both fundamental science and technological applications. For example, fission is a primary decay mechanism of superheavy elements [2] and plays a crucial role in the rapid neutron capture process at the origin of heavy elements in the universe [3]. Progress in these disciplines requires accurate and precise fission data, such as the distribution and full characteristics (charge, mass, excitation energy, spin, level density, etc.) of the fragments formed during the process. However, the ensemble of all these fissioning nuclei covers a vast area of the nuclear chart. While precise data are available on experimentally accessible nuclei, information on very short-lived, neutron-rich systems out of reach of experimental facilities must come from theoretical predictions.

There are many approaches geared toward describing low-energy neutron-induced fission reactions [4–12]. Among them, collective models have been particularly successful in predicting fission fragment distributions [3,10,13–19]. These models are based on the identification of a few collective variables driving the fission process, the calculation of a potential energy surface in the resulting collective space, and

the explicit time-dependent simulation of collective motion on top of these surfaces. Basic fission fragment properties such as proton or neutron number are mapped to the fissioning nucleus's characteristics, such as its deformation. Until now, particle-number estimates were obtained by simply integrating the density of particles in the prefragments. This local averaging made it impossible to predict fine structure effects such as the odd-even staggering in the fission fragments charge distributions.

In the seminal work of Refs. [20,21], the authors introduced a new method based on particle-number projection techniques to predict particle transfer in heavy-ion reactions in the context of time-dependent density functional theory. In Ref. [22], this method was applied to calculate the dispersion in particle number for the most probable scission configuration of $^{239}\text{Pu}(n, f)$ fission and showed that odd-even staggering naturally emerged. By further combining particle-number projection in the fission fragments with a strongly damped random walk on semiclassical potential energy surfaces, the authors of Ref. [23] showed that it is possible to predict odd-even staggering and also the charge polarization of the fission fragments' distribution.

This paper aims to combine particle-number projection in fission fragments with a quantum-mechanical theory of large-amplitude collective dynamics to predict the mass and charge fission fragment distributions before prompt emission. We investigate the role of projection for reproducing odd-even staggering effects in fragment distributions and discuss how various phenomenological probability distributions could approximate exact results. We also present the first two-dimensional isotopic yields predicted with such a

*verriere1@llnl.gov

microscopic approach and their evolution as a function of excitation energy.

In Sec. II, we describe in detail our theoretical framework. It includes a very short reminder on the time-dependent generator coordinate method under the Gaussian overlap approximation with Hartree-Fock-Bogoliubov (HFB) generator states, a comprehensive presentation of the method used to extract fission yields from the time evolution of a collective wave packet, and a discussion of the various methods to estimate particle-number dispersion in prefragments. Section III contains the results of our calculations for the two important cases of $^{235}\text{U}(n, f)$ and $^{239}\text{Pu}(n, f)$ low-energy fission, focusing on the impact of particle-number projection and the evolution of the yields as a function of excitation energy.

II. THEORETICAL FRAMEWORK

Our goal is to predict the initial, or primary, fission fragment mass and charge distributions before prompt emission of neutrons and gamma rays. These quantities are determined by estimating the population of scission configurations through the resolution of a collective Schrödinger-like equation in the collective space spanning nuclear deformations [6,24,25]. This approach is based on the time-dependent generator coordinate method (TDGCM) under the Gaussian overlap approximation (GOA). References [26,27] and references therein give a comprehensive presentation of the general framework; details about the specific implementation of the TDGCM + GOA for the description of fission dynamics can be found in Ref. [16].

In this section, we discuss in more detail our method to extract fission yields from TDGCM + GOA calculations by combining the population of scission configurations with an estimate of particle-number distributions at each configuration. We first recall in Sec. II A how we estimate the population of scission configurations in the TDGCM + GOA. We then derive in Sec. II B the expression for the probability distribution of the mass and charge of the fission fragments. These derivations require introducing the probability distributions associated with each scission configuration. The determination of the latter, based on particle-number projection techniques, is presented in Sec. II C.

A. Population of scission configurations

In practical applications, fission models that rely on the calculation of a potential energy surface (e.g., the semi-classical random walk and Langevin approaches or the fully-microscopic TDGCM) cannot correctly describe the separation of the fissioning nucleus into two separated and excited primary fragments; see Ref. [23] for further discussion. Instead, quantities such as fission fragment distributions are computed just before scission, which is defined, somewhat arbitrarily, based on several possible criteria; see discussions in Refs. [4,26].

Following common practice, we define scission configurations through the average value of the operator, \hat{Q}_N , counting the number of nucleons in the neck. It is defined, as in

Ref. [28], by

$$\hat{Q}_N = e^{-(z-z_N)^2/a_N^2}. \quad (1)$$

This expression contains two parameters. The neck location, z_N , is the point between the two prefragments along the z axis of the intrinsic reference frame where the local density is minimum. The position of the neck defines two prefragments: a point (x, y, z) belongs to the “left” fragment if $z < z_N$ and to the “right” fragment if $z \geq z_N$. The dispersion, a_N , is chosen to be equal to one nucleon. By convention, we consider that a configuration is located past scission, i.e., corresponds to two fully separated fragments, if

$$q_N \equiv \langle \phi(\mathbf{q}) | \hat{Q}_N | \phi(\mathbf{q}) \rangle \leq q_N^{\text{sciss}}, \quad (2)$$

where $|\phi(\mathbf{q})\rangle$ is the HFB state associated with the constrains $\mathbf{q} \equiv (q_{20}, q_{30})$ on the quadrupole and octupole moments and q_N^{sciss} is a parameter. This allows us to define the scission configurations as the set of all the states $|\phi(\mathbf{q})\rangle$ such that (i) $q_N > q_N^{\text{sciss}}$ and (ii) at least one of their neighbors is located past scission.

In our two-dimensional calculations, the set of scission configurations can be parametrized by a single coordinate ξ . The population of scission configurations is then obtained by integrating the flux density $\phi(\xi, t)$, which reads in this specific case

$$\phi(\xi, t) = J_0(\mathbf{q}(\xi), t) \frac{dq_1}{d\xi} - J_1(\mathbf{q}(\xi), t) \frac{dq_0}{d\xi}, \quad (3)$$

where $\mathbf{J} = (J_0, J_1)$ is the current as defined in Ref. [16]. We assume that the probability to exit through the point $\mathbf{q}(\xi)$ is proportional to the time-integrated flux density, defined as

$$F(\xi) = \lim_{t \rightarrow \infty} \int_{\tau=0}^{\tau=t} d\tau \phi(\xi, \tau). \quad (4)$$

B. Expression of the yields

Previous studies using the TDGCM framework to predict fission fragment yields accounted for the width of the particle-number probability distribution at a single scission configuration, as well as a possible experimental mass resolution (to compare with experimental preneutron yields), by convoluting the time-integrated flux density of Eq. (4) with a Gaussian function [16–19,29]. The mean of such a Gaussian is typically set to the average number of particles in the right fragment at the scission configuration $|\phi(\mathbf{q}(\xi))\rangle$, while its standard deviation is a free parameter. The major novelty of this work is the determination of the fission fragment mass and charge yields $Y(Z_f, A_f)$ by computing the exact probabilities for each fragment Z_f, A_f using a particle-number projection-based technique rather than a convolution with a Gaussian.

We seek to calculate the probability $\mathbb{P}(Z_R, N_R | Z, N)$ to measure Z_R charges and N_R neutrons in the right fragment at scission given a compound system with Z protons and N neutrons. In our approach, it is given by

$$\mathbb{P}(Z_R, N_R | Z, N) \propto \int d\xi F(\xi) \mathbb{P}(Z_R, N_R | Z, N, \mathbf{q}(\xi)), \quad (5)$$

where $\mathbb{P}(Z_R, N_R | Z, N, \mathbf{q}(\xi))$ is the probability, whose determination is presented in Sec. II C, associated with a right

fragment having Z_R protons and N_R neutrons, only considering the part of the compound system's state at $\mathbf{q}(\xi)$ having Z protons and N neutrons. Once this quantity is inserted in Eq. (5) and after a proper normalization, we recover the fission fragments yields, in percent, assuming that the system splits in two fragments:

$$Y(Z_f, N_f) = 100 \times [\mathbb{P}(Z_R = Z_f, N_R = N_f | Z, N) + \mathbb{P}(Z_R = Z - Z_f, N_R = N - N_f | Z, N)]. \quad (6)$$

We could use the same procedure to determine one-dimensional yields. For example, the charge distributions would read

$$Y(Z_f) = 100 \times [\mathbb{P}(Z_R = Z_f | Z, N) + \mathbb{P}(Z_R = Z - Z_f | Z, N)], \quad (7)$$

where the probability $\mathbb{P}(Z_R | Z, N)$, associated with Z_R protons in the right fragment at scission given Z and N , is

$$\mathbb{P}(Z_R | Z, N) \propto \int d\xi F(\xi) \mathbb{P}(Z_R | Z, N, \mathbf{q}(\xi)), \quad (8)$$

and the marginalized probability $\mathbb{P}(Z_R | Z, N, \mathbf{q})$ is given by

$$\mathbb{P}(Z_R | Z, N, \mathbf{q}) = \sum_{n=0}^N \mathbb{P}(Z_R, N_R = n | Z, N, \mathbf{q}). \quad (9)$$

However, all the distributions of interest can alternatively be obtained directly from $Y(Z_f, N_f)$ through the relations

$$Y(Z_f, A_f) = Y(Z_f, N_f = A_f - Z_f), \quad (10)$$

$$Y(Z_f) = \sum_{n=0}^N Y(Z_f, N_f = n), \quad (11)$$

$$Y(A_f) = \sum_{n=0}^N Y(Z_f = A_f - n, N_f = n). \quad (12)$$

Therefore, the essential quantity to compute the fission yields is the probability distribution $\mathbb{P}(Z_R, N_R | Z, N, \mathbf{q})$.

C. Particle-number projection

In this work, we estimate the distribution of probability $\mathbb{P}(Z_R, N_R | Z, N, \mathbf{q})$ based on particle-number projection techniques. Particle-number projection (PNP) was originally introduced to restore the number of particles in superfluid systems that spontaneously break the particle-number symmetry [30–34]. Following Refs [20–22], we use PNP to estimate the probability $\mathbb{P}(Z_R, N_R | Z, N, \mathbf{q})$. For a fissioning nucleus described by the many-body state $|\phi(\mathbf{q})\rangle$, this value can be interpreted as the probability to measure Z_f protons and N_f neutrons in the right fragment in the component of $|\phi(\mathbf{q})\rangle$ with Z protons and N neutrons.

We do not consider isospin mixing in this work, i.e.,

$$|\phi(\mathbf{q})\rangle = |\phi(\mathbf{q})\rangle_{\text{neut.}} \otimes |\phi(\mathbf{q})\rangle_{\text{prot.}} \quad (13)$$

Thus, the probabilities $\mathbb{P}(Z_R, N_R | Z, N, \mathbf{q})$ can be decomposed accordingly,

$$\mathbb{P}(Z_R, N_R | Z, N, \mathbf{q}) = \mathbb{P}(N_R | N, \mathbf{q}) \times \mathbb{P}(Z_R | Z, \mathbf{q}). \quad (14)$$

The probability distributions $\mathbb{P}(Z_R | Z, \mathbf{q})$ and $\mathbb{P}(N_R | N, \mathbf{q})$ both derive from a double projection of the scission configuration $|\phi(\mathbf{q})\rangle$:

$$\mathbb{P}(Z_R | Z, \mathbf{q}) = \frac{\langle \phi(\mathbf{q}) | \hat{P}_p^{(R)}(Z_R) \hat{P}_p(Z) | \phi(\mathbf{q}) \rangle}{\langle \phi(\mathbf{q}) | \hat{P}_p(Z) | \phi(\mathbf{q}) \rangle}. \quad (15)$$

The operator $\hat{P}_p(Z)$ projects the state onto the states' eigenspace with a good total proton number Z . We implemented this projector in its standard gauge angle integral form

$$\hat{P}_p(Z) = \frac{1}{2\pi} \int_0^{2\pi} d\theta e^{i\theta(\hat{Z}-Z)}. \quad (16)$$

Similarly, the operator $\hat{P}_p^{(R)}(Z_R)$ projects onto the eigenspace of states with a good number of protons Z_R in the right half-space. We recall that the right half-space corresponds to the set of spatial coordinates whose component along the z axis is greater than z_N , the position of the neck. Its expression reads

$$\hat{P}_p^{(R)}(Z_R) = \frac{1}{2\pi} \int_0^{2\pi} d\theta e^{i\theta(\hat{Z}_R - Z_R)}, \quad (17)$$

where \hat{Z}_R counts the number of protons in the right half-space. This operator can be expressed from the proton creation, $\hat{a}^{(p)\dagger}(\mathbf{r}, \sigma)$, and annihilation, $\hat{a}^{(p)}(\mathbf{r}, \sigma)$, operators as

$$\hat{Z}_R = \sum_{\sigma=\downarrow, \uparrow} \int_x \int_y \int_{z=z_N}^{+\infty} d\mathbf{r} \hat{a}^{(p)\dagger}(\mathbf{r}, \sigma) \hat{a}^{(p)}(\mathbf{r}, \sigma). \quad (18)$$

We define the projectors on the neutrons number, in the full space, $\hat{P}_n(N)$, as well as in the right half-space, $\hat{P}_n^{(R)}(N_R)$, in a similar way, and we follow the same procedure to calculate the neutron probability

$$\mathbb{P}(N_R | N, \mathbf{q}) = \frac{\langle \phi(\mathbf{q}) | \hat{P}_n^{(R)}(N_R) \hat{P}_n(N) | \phi(\mathbf{q}) \rangle}{\langle \phi(\mathbf{q}) | \hat{P}_n(N) | \phi(\mathbf{q}) \rangle}. \quad (19)$$

In our calculations, we determine the numerator of Eqs. (15) and (19) using the gauge angle integrals based on a Fomenko quadrature [35] using 41 integration points. Instead of explicitly calculating the corresponding denominator, we directly normalize the distributions using

$$\langle \phi(\mathbf{q}) | \hat{P}_p(Z) | \phi(\mathbf{q}) \rangle = \sum_z \langle \phi(\mathbf{q}) | \hat{P}_p^{(R)}(z) \hat{P}_p(Z) | \phi(\mathbf{q}) \rangle, \quad (20)$$

$$\langle \phi(\mathbf{q}) | \hat{P}_n(N) | \phi(\mathbf{q}) \rangle = \sum_n \langle \phi(\mathbf{q}) | \hat{P}_n^{(R)}(n) \hat{P}_n(N) | \phi(\mathbf{q}) \rangle. \quad (21)$$

III. APPLICATION

This section summarizes our results for the thermal neutron-induced fission of ^{235}U and ^{239}Pu . In Sec. III A, we discuss the static fission properties related to the potential energy surfaces and the properties of prefragments at scission. In Sec. III B, we show the primary fission fragments mass and charge yields obtained by combining the TDGCM + GOA collective dynamics with PNP. We then compare the projected yields with results obtained from assuming several analytical distributions in Sec. III C, and assuming different criteria for the scission line in Sec. III D. Finally, the evolution of both the

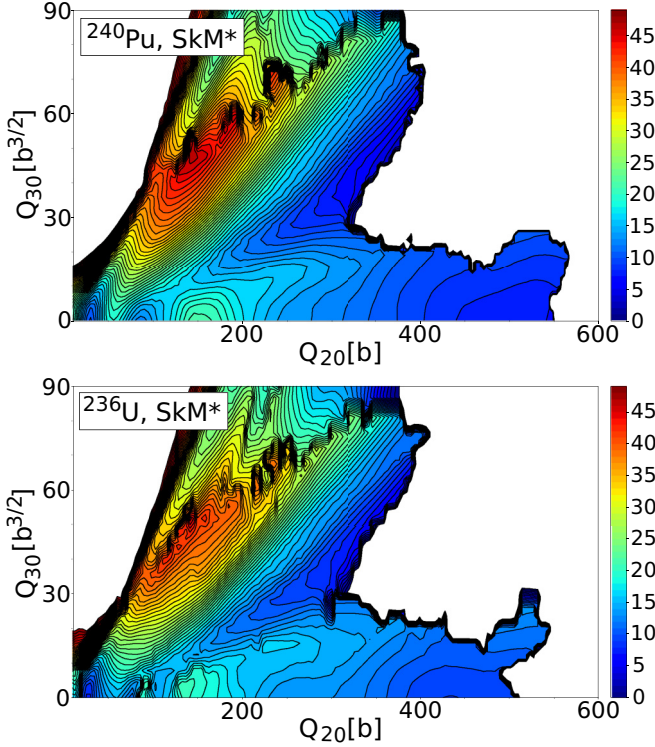


FIG. 1. Potential energy surface for ^{240}Pu (top) and ^{236}U (bottom) as a function of the axial quadrupole and axial octupole moments.

two-dimensional yields and their one-dimensional reductions as a function of the energy of the incident neutron is illustrated in Sec. III E.

A. Static properties

While the potential energy surfaces (PESs) used in this work have already been presented in other publications—Ref. [36] for ^{240}Pu and Ref. [37] for ^{236}U —we recall them for the sake of completeness. Figure 1 thus shows the total potential energy $V(\mathbf{q})$ entering the master equation of the TDGCM + GOA, namely Eq. (4) of Ref. [16], for both ^{240}Pu (top) and ^{236}U (bottom) as a function of the axial quadrupole and octupole moments. The PES is characterized by a ground-state at around $Q_{20} \approx 30$ b, a fission isomer at $Q_{20} \approx 85$ b, and the main large fission valley opening up beyond the second barrier. Note that triaxiality is included in this calculation, but plays a role only near the first barrier; see Ref. [36] for a discussion. Additional details about the resolution of the HFB equation, such as the characteristics of the harmonic oscillator basis or the convention for the multipole operators used as constraints can be found in that same reference.

An HFB generator state $|\phi(\mathbf{q})\rangle$ is associated with each point of the PES of Fig. 1. The scission configurations are defined based on the procedure outlined in Sec. II. For each state in the scission region, we identify the neck position z_N , which is used to compute the average charge, number of

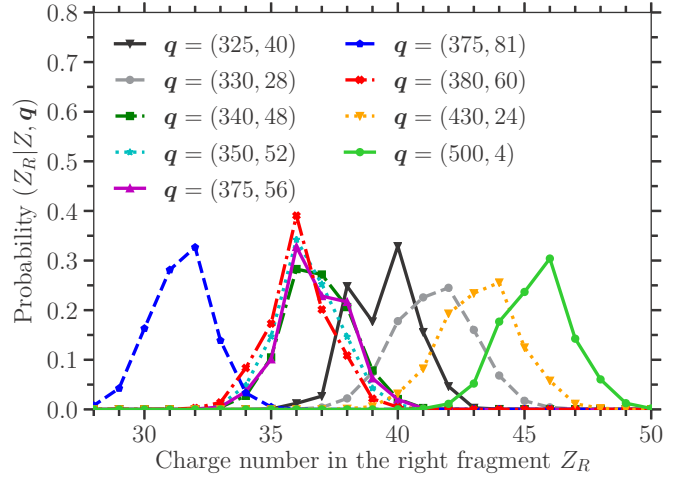


FIG. 2. Probability $\mathbb{P}(Z_R | Z, \mathbf{q})$ of having Z_R protons in the right fragment given the total number of protons Z as a function of Z_R . We show such a probability distribution for a set of scission configurations \mathbf{q} in ^{236}U . The deformations \mathbf{q} are in b (q_{20}) and $b^{3/2}$ (q_{30}), where $b = \text{barn}$.

neutron, and mass, according to

$$\langle \hat{Z}_R \rangle = \int_{-\infty}^{+\infty} dx \int_{-\infty}^{+\infty} dy \int_{z_N}^{+\infty} dz \rho_p(\mathbf{r}), \quad (22)$$

$$\langle \hat{N}_R \rangle = \int_{-\infty}^{+\infty} dx \int_{-\infty}^{+\infty} dy \int_{z_N}^{+\infty} dz \rho_n(\mathbf{r}), \quad (23)$$

$$\langle \hat{A}_R \rangle = \int_{-\infty}^{+\infty} dx \int_{-\infty}^{+\infty} dy \int_{z_N}^{+\infty} dz \rho_0(\mathbf{r}), \quad (24)$$

where ρ_n and ρ_p are respectively the neutron and proton density distributions and $\rho_0 = \rho_n + \rho_p$ is the isoscalar (total) density. Since the HFB wave function is not an eigenstate of the operator of Eq. (18) counting the number of particles in the right fragment, the fluctuations $\langle \hat{Z}_R^2 \rangle$ and $\langle \hat{A}_R^2 \rangle$ are nonzero and could be in principle computed as well.

Projection techniques give us a much more complete view of the content in particle number in the fragments. For each scission configuration of the two PES we performed the projection on the total number of protons and neutrons as well as on the number of protons and neutrons in the right half-space following Eq. (15). The projection on the fragment particle numbers was only performed for eigenvalues Z_R and N_R close to the mean values defined by Eq. (22), where the probability is not negligible. In practice we considered in each scission configuration the set $\lfloor \langle \hat{Z}_R \rangle \rfloor - 20 \leq Z_R < \lfloor \langle \hat{Z}_R \rangle \rfloor + 20$ and $\lfloor \langle \hat{N}_R \rangle \rfloor - 20 \leq N_R < \lfloor \langle \hat{N}_R \rangle \rfloor + 20$, hence a total of 41 projected values for protons and for neutrons. The notation $\lfloor X \rfloor$ indicates the integer part of the real number X .

Figure 2 presents an example of these probabilities distributions for the case of a few scission configurations in ^{236}U , the locations \mathbf{q} of which are indicated in the legend. More specifically, it shows the probability $\mathbb{P}(Z_R | Z, \mathbf{q})$ as a function of the charge number Z_R for the fixed value $Z = 92$ of the total number of proton in the fissioning nucleus. These results highlight two important features brought about by projection:

(i) the curves are not necessarily symmetric around the mean value and (ii) there can be odd-even staggering effects, as in the case of the configuration $(q_{20}, q_{30}) = (325 \text{ b}, 40 \text{ b}^{3/2})$. These two features are absent by construction when considering empirical dispersion laws such as Gaussian folding.

B. Fragment distributions

In this section, we show the primary mass and charge distributions for the two important cases of the low-energy, neutron-induced fission of ^{235}U and ^{239}Pu . Throughout this section, FELIX calculations were performed with the GCM collective inertia, the metric $\gamma(\mathbf{q})$ and the GCM zero point energy correction, and the frontier was defined by $q_N^{\text{sciss}} = 4.0$. The dispersion in energy of the initial collective wave packet, see Eq. (19) of Ref. [16], is $\sigma = 0.5 \text{ MeV}$. The collective dynamics with FELIX is characterized by a time step of $\Delta t = 2 \times 10^{-4} \text{ zs}$ and we simulate the dynamics up to a time $t = 20 \text{ zs}$.

For the two actinides under consideration, there are considerably fewer measurements on charge distributions $Y(Z)$ than on mass distributions $Y(A)$. Yet charge distributions are important tests for theory since they can exhibit an odd-even effect, namely, the yield of even- Z elements is higher than that of odd- Z [40–44]. Note that an experimental determination of such an effect requires a sufficiently good resolution in the detection of the fragment charge. Typically, for the case of neutron-induced fission of ^{235}U at thermal energy, odd-even effects were not reported in [38]. According to the authors, the experimental technique used as well as the hypothesis assumed in the data analysis could smooth out the odd-even structures in this work. In contrast, the experiment of Ref. [39] claims a resolving power of $Z/\Delta Z = 45$ (full width at 1/10 maximum) for the charge $Z = 40$ at the maximum of the light peak. With such resolution, the resulting yields present a strong odd-even staggering effect. Such effect was also observed for various fissioning systems in the high precision measurements based on inverse kinematics reactions at higher excitation energies [45–47].

In Fig. 3, we show the charge distributions for the neutron-induced fission $^{239}\text{Pu}(n, f)$ and $^{235}\text{U}(n, f)$ reactions, at an excitation energy of 1 MeV above the first fission barrier. For these fissile isotopes it should correspond to an incident neutron energy of $E_n \simeq 1 \text{ MeV}$. For both systems, the overall agreement with data is satisfactory, especially considering the lack of precise experimental measurements of charge distributions for the ^{240}Pu . In the case of ^{236}U , it is worth noting that our calculations do not predict odd-even effects in the charge yields. We will discuss this in more details in Sec. III D.

In Fig. 4, we show the mass distributions for these same isotopes. The agreement with data is not as good, especially in the case of $^{235}\text{U}(n, f)$. However, we must bear in mind that these experimental primary mass yields do not have a perfect mass resolution. The mass of the (primary) fragments is typically deduced from the measurement of the kinetic energy of the fission fragments in ionization chambers. This technique implies a mass resolution of roughly $\text{FWHM} = 5.5$ mass units for A [57]. Therefore, we also show in Fig. 4 the

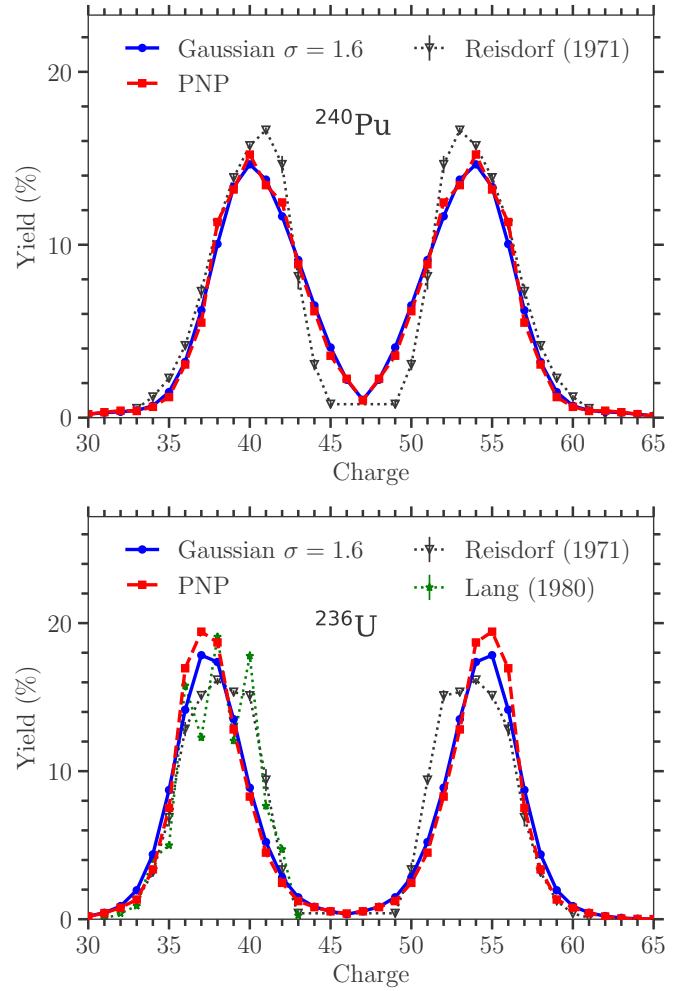


FIG. 3. Charge distribution $Y(Z)$ in ^{240}Pu (top) and ^{236}U (bottom) as a function of Z . The yields obtained with PNP are compared to a Gaussian convolution of the raw flux with $\sigma = 1.6$ and to the experimental data from Refs. [38,39]; see text for additional details.

results of the calculation when accounting for such a mass resolution.

In both Figs. 3 and 4, we compare the theoretical calculations with PNP with the standard method of Gaussian folding. Note that the width σ of the folding must be different for protons and for masses as the overall proton density is smaller than the total one. As a result, most of the (theoretical) uncertainty on the proton number can be attributed to pairing effects in each prefragment. As seen in Fig. 2, the average dispersion around the mean value is of the order of 1.6 indeed. In contrast, neutrons are much less localized in the prefragments and contribute rather significantly to the overall neck between the prefragments [36,58,59]. The number of particles in the neck used to define scission configuration in our calculations, $q_N^{\text{sciss}} = 4.0$, is larger than the typical dispersion in particle number one could expect from pairing effects and thus dominates. This justifies fixing $\sigma = 4$ for the Gaussian folding of mass yields. It is worth mentioning that, for this reference calculation at $q_N^{\text{sciss}} = 4.0$, Gaussian folding is a very good approximation to the exact PNP result. In Sec. III C we

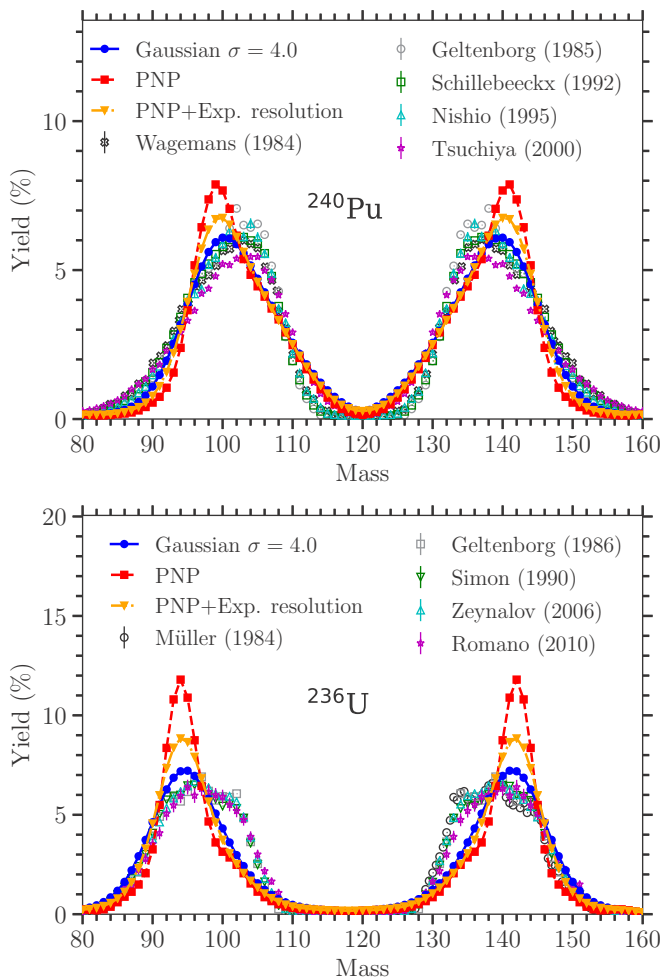


FIG. 4. Mass distribution $Y(A)$ in ^{240}Pu (top) and ^{236}U (bottom) as a function of A . Results obtained after PNP are compared to a Gaussian convolution of the raw flux with $\sigma = 4.0$ and to experimental data from Refs. [48–56]. The curve labeled PNP + Exp. resolution gives the PNP results with an additional convolution by a Gaussian with a FWHM of 5.5 mass units to account for the typical mass resolution of experiments; see text for additional details.

will evaluate the performance of other analytical probability laws, and in Sec. III D we will further discuss the dependency of the results on the definition of the frontier.

Beyond enhancing the robustness of our approach by eliminating the (somewhat) arbitrary width of the Gaussian folding, PNP also allows determining more realistic two-dimensional isotopic distribution $Y(Z, A)$. Such distributions are especially important when simulating the deexcitation of fission fragments [60]. The results for the particular case of ^{240}Pu are presented in Fig. 5. To our knowledge, no experimental data can be directly compared to these preneutron emission yields. Thus, we present the two-dimensional independent yields (after the emission of the prompt neutrons) of the JEFF-3.3 evaluated data library [61] alongside our results. We show that the PNP approach predicts a significant width for the light and heavy peaks of the two-dimensional fission yields. This width is larger than the data of JEFF-3.3. Currently, it is not clear

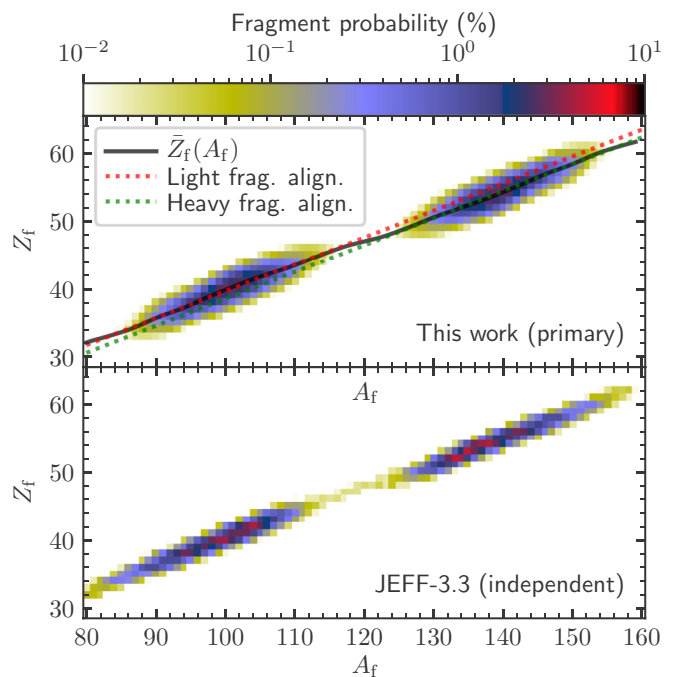


FIG. 5. Two-dimensional isotopic fission yields $Y(Z, A)$ for the reaction $^{239}\text{Pu}(n, f)$ for an incoming neutron energy of $E_n = 1.0$ MeV using PNP in the fragments. Our results predict a deviation from the unchanged charge distribution (UCD) approximation, called the charge-polarization of the fission fragment distributions, in the primary yields. To give a point of reference, we also show the independent two-dimensional yields evaluated in the JEFF-3.3 library. Note that these yields account for the mass number of the fragments after emission of the prompt neutrons (in contrast to our predictions that give the primary fragment yields).

whether this reduction of the width could be totally explained by the prompt neutron emission.

From $Y(Z_f, A_f)$ we can extract the charge polarization ΔZ_f which measures the deviation of the most probable charge in a fragment of given mass to the unchanged charge distribution (UCD) approximation [62],

$$\Delta Z_f(A_f) = \bar{Z}_f(A_f) - A_f \frac{Z}{A}, \quad (25)$$

with

$$\bar{Z}_f(A_f) = \frac{\sum_{Z_f} Z_f \times Y(Z_f, A_f)}{\sum_{Z_f} Y(Z_f, A_f)}. \quad (26)$$

For the thermal neutron induced-fission induced on ^{239}Pu , a large corpus of experimental data agree on a charge polarization of the order of -0.5 charge unit for the heavy fragments [63,64]. We find in this work a consistent value of -0.58 on average on the fragments in the heavy peak ($A_f \in [130, 150]$). A qualitative explanation of this polarization effect, already proposed in 1966 [65], is the asymmetry energy term in the liquid drop formula of the deformation energy. However, no such preneutron experimental data were available at the time. As illustrated in Ref. [66], classical models are able to explain the smooth trend of the charge polarization favoring less protons in the heavy fragment. On top of that, shell and pairing

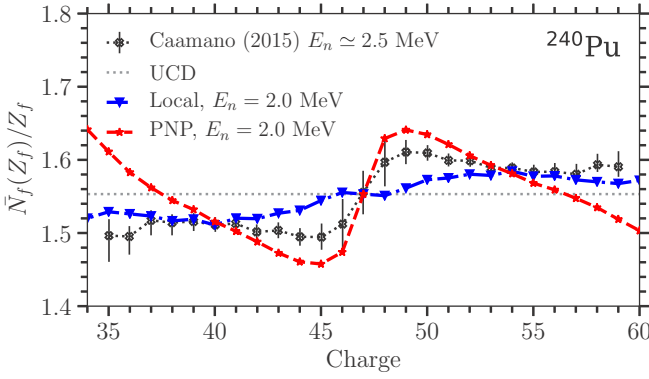


FIG. 6. Average neutron excess of fragments produced in the fission of ^{240}Pu . PNP results at $E_n = 2.0$ MeV are compared with the local discrete approach of Sec. III C and with the experimental data of Ref. [66].

effects bring additional structures to the charge polarization measured in the fission of actinides in general [67,68].

An equivalent probe for this phenomenon is the neutron excess, defined as

$$\frac{\bar{N}_f(Z_f)}{Z_f} = \frac{\sum_{N_f} N_f/Z_f \times Y(Z_f, N_f)}{\sum_{N_f} Y(Z_f, N_f)}. \quad (27)$$

We compare in Fig. 6 the predictions of the TDGCM dynamics with PNP to the experimental data obtained with the VAMOS spectrometer [66]. The experimental data come from an inverse kinematic experiment with an equivalent incident neutron energy of $\simeq 2.5$ MeV and a standard deviation of 6 MeV on this energy. To obtain an approximate description of this entrance channel, we performed our calculation with an initial energy of 2 MeV above the first fission barrier. The shape of the neutron excess obtained, especially the bump when going from the light to the heavy fragment and the overall order of magnitude in the light and heavy fragments, reproduces well this experimental data set. At high asymmetries we notice significant deviations from experiment. To see the impact of projection on the quality of our prediction we also show the results obtained when the two-dimensional mass and charge yields are simply estimated with the local discrete approach of Sec. III C. Particle-number projection turns out to be an important ingredient for reproducing the neutron excess.

C. Comparison with various analytical distributions

Many studies of fission fragment distributions in the framework of the TDGCM + GOA approximate the uncertainty on particle number at scission, or equivalently, particle transfer effects, by simple Gaussian folding of the mean value of particles for each scission configuration [16–19,29,69]. This corresponds to setting the quantity $\mathbb{P}(Z_R, N_R | Z, N, \mathbf{q}(\xi))$ involved in Eq. (5) to follow a Gaussian distribution as discussed in Sec. III C. In the work of Ref. [70], this convolution of the flux was also obtained from a random neck rupture mechanism.

In this section, we compare fission distributions obtained through the direct calculation of the projected mass and charge

of the fragments with the ones obtained assuming analytic probability distributions for $\mathbb{P}(Z_R, N_R | Z, N, \mathbf{q})$. For each distribution, the mean μ is set to the average number of particles (neutrons or protons) in the fragments. Note that this slightly differs from our previous works, see Ref. [16,18], where μ was chosen to be the closest integer to the average number of particles.

The first analytical distribution we consider is the Gaussian distribution used in earlier works and also used to add a mass resolution in the fission fragment distribution before comparing with experimental data [71]. While the mean of this distribution is specified by the average number of particles, the standard deviation σ is a free parameter. The contribution of a scission configuration is then

$$\begin{aligned} \mathbb{P}(Z_R | Z, N, \mathbf{q}) &= \frac{1}{2} \operatorname{erf} \left(\frac{Z_R + \frac{1}{2} - \mu(\mathbf{q})}{\sqrt{2}\sigma} \right) - \frac{1}{2} \operatorname{erf} \left(\frac{Z_R - \frac{1}{2} - \mu(\mathbf{q})}{\sqrt{2}\sigma} \right). \end{aligned} \quad (28)$$

The hypothesis that the dispersion in charge number Z_R in the fission fragments is minimal leads to the second distribution considered in this paper, the *most local distribution* of mean μ . The domain of this distribution is the set of positive integers. The only integers associated with a nonzero probability are $\lfloor \mu \rfloor$ and $\lfloor \mu \rfloor + 1$, respectively having the probabilities $1 - x$ and x , where $x = \mu - \lfloor \mu \rfloor$. Consequently, the contribution $\mathbb{P}(Z_R, N_R | Z, N, \mathbf{q})$ reads

$$\mathbb{P}(Z_R | Z, N, \mathbf{q}) = \begin{cases} 1 - x & \text{if } X_f = \lfloor \mu(\mathbf{q}) \rfloor, \\ x & \text{if } X_f = \lfloor \mu(\mathbf{q}) \rfloor + 1, \\ 0 & \text{otherwise.} \end{cases} \quad (29)$$

If we model scission as a set of independent and identically distributed draws where each nucleons is put in the left or right fragment according to a coin toss, the probability distribution follows a binomial law:

$$\mathbb{P}(Z_R | Z, N, \mathbf{q}) = \binom{X}{X_f} (\mu/X)^{X_f} [1 - (\mu/X)]^{X - X_f}. \quad (30)$$

Finally, the law of rare events suggests that the more asymmetrical fission is, the better the binomial law can be approximated by the fourth and last distribution considered in this work, a Poisson distribution whose contribution at each point \mathbf{q} is

$$\mathbb{P}(Z_R | Z, N, \mathbf{q}) = \frac{\mu^{X_f} e^{-\mu}}{X_f!}. \quad (31)$$

The results are summarized in Fig. 7 for the charge yields; the mass yields are qualitatively similar. The Poisson and binomial distributions are considerably too broad. In contrast, both the local discrete and Gaussian distribution do a decent job at reproducing the width of the charge distribution, although the local discrete distribution is too narrow, leading to overestimating the height of the peaks. The fact that a Gaussian convolution reproduces quite well the PNP is consistent with the conclusions of Ref. [72], although they were obtained in a different context where the projection subvolume is spherical.

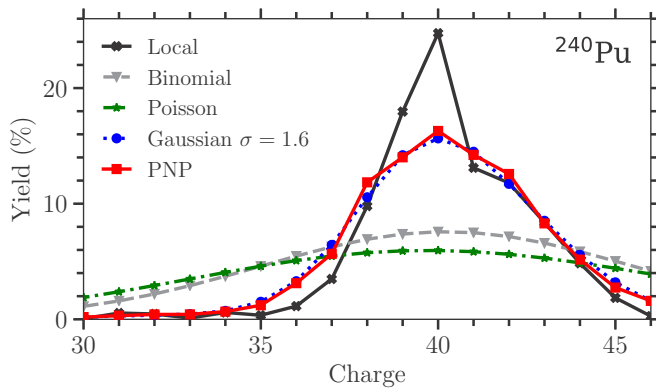


FIG. 7. Light peak of the charge distribution $Y(Z)$ in ^{240}Pu as a function of Z for different analytic forms for $\mathbb{P}(Z_R, N_R | Z, N, q)$ as well as from PNP. We only show the curve for the light fragment, since the whole distribution is completely symmetric with respect to $Z/2$; see text for additional details.

D. Evolution of yields as function of frontier definition

One of the well-known limitations of adiabatic approaches to fission is the dependency of results on the definition of scission configurations [4,58,73]. This problem is especially relevant in self-consistent HFB calculations of PES: the large computational cost often leads to limiting the number of active collective variables—two in our case—which leads to discontinuities in the PES [74]. Very often, scission configurations are in fact associated with such a major discontinuity. In Fig. 1, the line that separates the colored area from the white background at $q_{20} > 300$ b is the visual representation of such a discontinuity, where the expectation value q_N of the Gaussian neck operator drops from 3–6 down to values smaller than 0.1. It is especially important to quantify the impact of the definition of the frontier on charge distributions, as recent work suggests the odd-even staggering effect may only manifest itself at rather small values of the neck between the two prefragments [23].

In Fig. 8, we thus show the evolution of the charge distribution in ^{240}Pu as a function of the criterion q_N^{sciss} used to define scission configurations, as explained in Sec. II A. As expected, there is no evidence of odd-even staggering for large values of q_N . For $3.0 \leq q_N \leq 8.0$, the peak does not really change very significantly. The first hints of odd-even staggering only appear at $q_N \leq 2.5$. At the same time, there is a more pronounced shift of the peak toward larger values of Z . While this result is encouraging, we should point out that values of $q_N < 3$ often require interpolating the PES through the discontinuity defining scission, which is non physical. Better-resolved, continuous PESs are required to verify the possibility of an odd-even staggering effects. This may be achieved for instance by increasing the number of collective degrees of freedom.

E. Evolution of yields as function of excitation energy

Within our approach, we can estimate the primary fission fragment mass and charge distributions $Y(A; E_n)$ and $Y(Z; E_n)$ for different values of the incoming neutron energy E_n . For

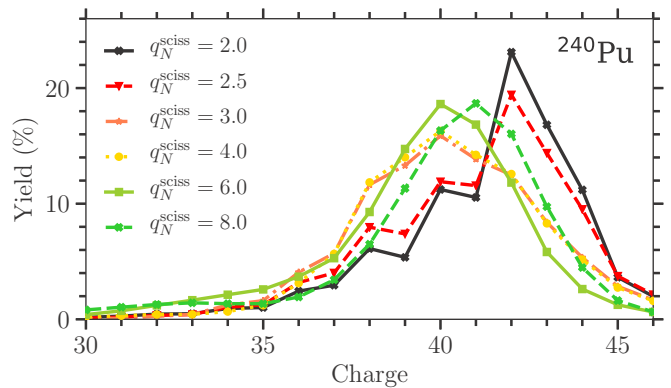


FIG. 8. Light peak of the fragment charge distribution $Y(Z)$ in ^{240}Pu at $E_n = 1.0$ MeV obtained with different values of the frontier definition q_N^{sciss} .

this purpose, we make the approximation that all the excitation that the compound nucleus acquires after absorbing the neutron is of collective nature. This implies that varying incident neutron energies E_n translate simply into varying mean energies of the collective wave packet; see Eq. (19) of Ref. [16]. We are very aware that this approximation is rather strong and probably not entirely valid. A more accurate treatment of collective dynamics would require including quasiparticle excitations in the TDGCM formalism along the lines of Ref. [75], or adopting a finite-temperature approach as in, e.g., Refs. [29,76]. The former strategy faces considerable computational challenges, while the latter is not formally well defined: the very concept of a GCM wave function made of a superposition of kets requires generalization at finite temperature; see, e.g., Ref. [77]. Pending such future developments and bearing in mind the limitations of our approach, we can still provide a useful reference point for future comparisons.

In Fig. 9, we thus show the evolution of the full, two-dimensional isotopic fragment distribution as a function of incident neutron energy. As expected from statistical mechanics—at “infinite” excitation energy, all fragmentations should become equiprobable—the distribution $Y(Z, A; E_n)$ includes an ever larger set of fragmentations as the incident neutron energy increases from $E_n = 0.5$ MeV to $E_n = 10.0$ MeV. In particular, symmetric fission becomes more and more likely, which is especially visible for $E_n > 3.0$ MeV, and very asymmetric configurations with $A_L \approx 80$ get more and more populated. A more careful analysis of these maps show that the centroid of the distribution for the light fragment shifts toward lower Z_L and lower A_L : at $E_n = 0.5$ MeV, it is located at $(Z_L, A_L) = (39.875, 100.364)$ and has moved to $(Z_L, A_L) = (37.987, 95.575)$ at $E_n = 10.0$ MeV. Similarly the most likely fission fragment changes from ^{100}Zr ($Z_L = 40, N_L = 60$) at $E_n = 0.5$ MeV to ^{96}Sr ($Z_L = 37.987, A_L = 95.575$) at $E_n = 10.0$ MeV.

To get a more quantitative feel for the variations of individual charge yields, we show in Fig. 10 the charge yields of ^{240}Pu for various incident neutron energies in the range $E_n \in [0.5; 10]$ MeV. These results are compared to the experimental data of Ramos *et al.* [46] obtained in inverse kinematics. This experiment leverages the transfer reaction

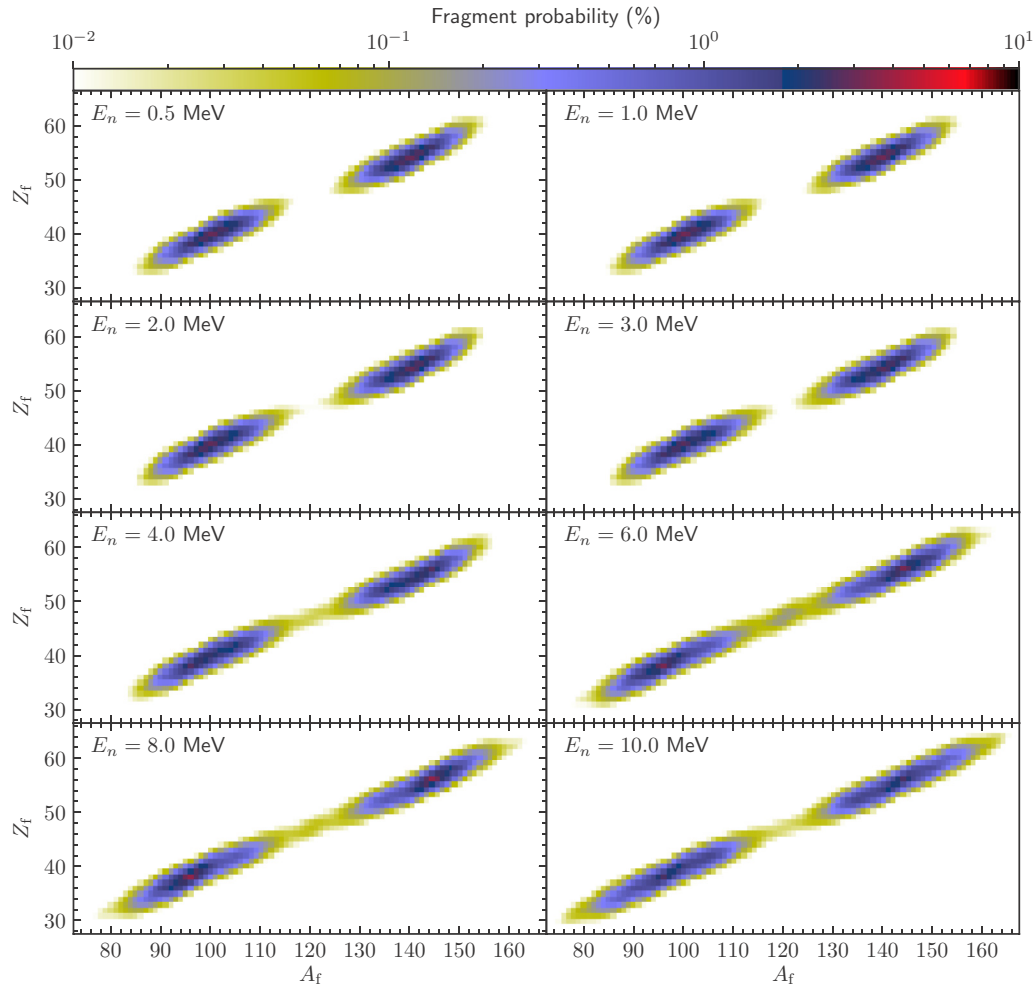


FIG. 9. Isotopic yields $Y(Z_f, A_f)$ for the reaction $^{239}\text{Pu}(n, f)$ for different incoming neutron energies E_n using PNP in the fragments. Symmetric fission becomes more probable with increasing excitation energy.

$^{12}\text{C}(^{238}\text{U}, ^{240}\text{Pu})^{10}\text{Be}$ to produce the compound plutonium system with an average excitation energy of 10.7 MeV and a standard deviation of 3.0 MeV. This energy corresponds to an incident neutron energy of $E_n = E^* - S_n \simeq 4.3$ MeV,

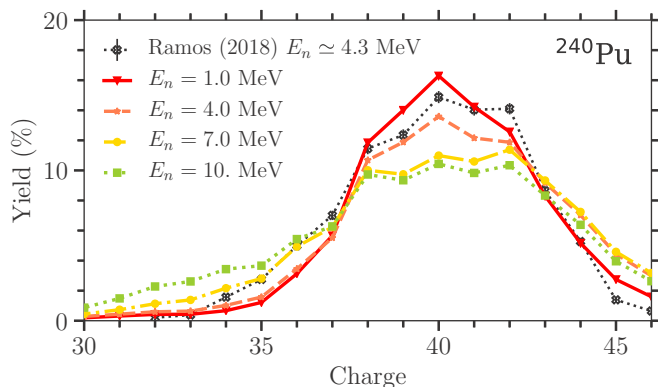


FIG. 10. Light peak of the fragment charge distribution $Y(Z)$ for ^{240}Pu obtained with different values of initial energy of the compound nucleus. Results with PNP are compared to the experimental data from Ref. [46].

although differences in the resulting fission yields may arise from the difference of input reaction channel. Once again our results show a broadening of the charge yields with the increase of the neutron energy. Overall, our predictions at $E_n = 4$ MeV compare well with the experimental data of Ref. [46]. We still notice a strong overestimation of the predicted charge yields in the symmetric valley.

Finally, Fig. 11 shows the evolution of the neutron excess of Eq. (27) as a function of incident neutron energy. We see that the addition of the excitation energy to the system tends to flatten the structure of the neutron excess. These predictions are qualitatively consistent with the observed fission of ^{250}Cf at high excitation energy ($E^* = 43$ MeV) [66] as well as with the interpretation of shell effects being smoothed out as the energy increases.

IV. CONCLUSION

In this paper, we reported the first microscopic calculation of fission fragment distribution within the TDGCM + GOA framework where the number of particles in fission fragments was extracted by direct particle-number projection. While using Gaussian folding of particle number at scission

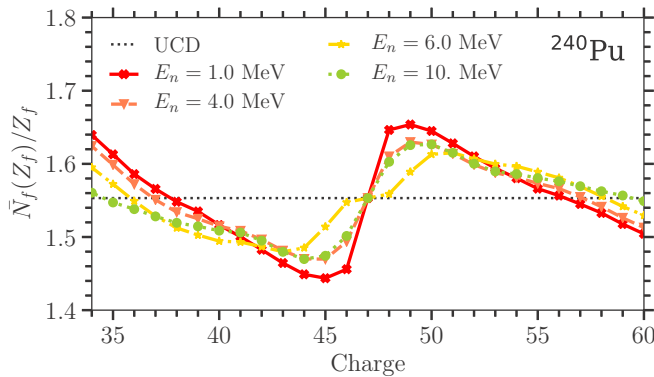


FIG. 11. Evolution of the neutron excess of the primary fission fragments for the reaction $^{239}\text{Pu}(n, f)$ according to E_n . If the UCD were satisfied, all these quantities would be constant equal to 1.55.

is a good approximation of the exact PNP result, it still requires specifying the width. Even guided by consideration about pairing fluctuations or the size of the neck, this parameter remains somewhat arbitrary; PNP techniques allow eliminating it entirely and thereby obtaining more realistic distributions.

When comparing with experimental data for the two standard cases of ^{236}U and ^{240}Pu , we find that the agreement on both charge and mass yields is satisfactory, especially considering the rather large uncertainties on the primary fragment

distributions, which translates itself into a large experimental mass resolution for the mass yields, and somewhat conflicting datasets for the charge yields. Our analysis of the two-dimensional isotopic yields recovers the expected charge polarization already at the level of the primary yields, i.e., before any evaporation of neutrons. Many recent measurements seem to confirm the existence of an odd-even staggering in the charge distributions. Our calculations with small neck sizes for scission configurations seem to confirm this, although the resolution of the potential energy surface is not sufficient to draw firm conclusions.

The evolution of the yields as a function of incident neutron energy, which in our framework translates into collective excitation energy of the fissioning nucleus, is compatible with what is expected from statistical mechanics and observed experimentally: the peaks of the distribution widen and symmetric fission increases. We note that the shell effects visible on the predicted charge polarization tend to vanish with increasing energy.

ACKNOWLEDGMENTS

This work was supported in part by the NUCLEI SciDAC-4 collaboration DE-SC001822 and was performed under the auspices of the U.S. Department of Energy by Lawrence Livermore National Laboratory under Contract No. DE-AC52-07NA27344. Computing support came from the Lawrence Livermore National Laboratory (LLNL) Institutional Computing Grand Challenge program.

- [1] M. Bender, R. Bernard, G. Bertsch, S. Chiba, J. Dobaczewski, N. Dubray, S. A. Giuliani, K. Hagino, D. Lacroix, Z. Li, P. Magierski, J. Maruhn, W. Nazarewicz, J. Pei, S. Péru, N. Pillet, J. Randrup, D. Regnier, P.-G. Reinhard, L. M. Robledo *et al.*, Future of nuclear fission theory, *J. Phys. G: Nucl. Part. Phys.* **47**, 113002 (2020).
- [2] A. Baran, M. Kowal, P.-G. Reinhard, L. M. Robledo, A. Staszczak, and M. Warda, Fission barriers and probabilities of spontaneous fission for elements with $Z \geq 100$, *Nucl. Phys. A* **944**, 442 (2015), Special Issue on Superheavy Elements.
- [3] M. R. Mumpower, P. Jaffke, M. Verriere, and J. Randrup, Primary fission fragment mass yields across the chart of nuclides, *Phys. Rev. C* **101**, 054607 (2020).
- [4] N. Schunck and L. M. Robledo, Microscopic theory of nuclear fission: A review, *Rep. Prog. Phys.* **79**, 116301 (2016).
- [5] D. G. Madland and J. Nix, New model of the average neutron and proton pairing gaps, *Nucl. Phys. A* **476**, 1 (1988).
- [6] J. Berger, M. Girod, and D. Gogny, Time-dependent quantum collective dynamics applied to nuclear fission, *Comput. Phys. Commun.* **63**, 365 (1991).
- [7] Y. Tanimura, D. Lacroix, and S. Ayik, Microscopic Phase-Space Exploration Modeling of ^{258}Fm Spontaneous Fission, *Phys. Rev. Lett.* **118**, 152501 (2017).
- [8] A. Bulgac, P. Magierski, K. J. Roche, and I. Stetcu, Induced Fission of ^{240}Pu within a Real-Time Microscopic Framework, *Phys. Rev. Lett.* **116**, 122504 (2016).
- [9] P. Möller, A. Sierk, T. Ichikawa, and H. Sagawa, Nuclear ground-state masses and deformations: FRDM(2012), *At. Data Nucl. Data Tables* **109-110**, 1 (2016).
- [10] H. Goutte, J. F. Berger, P. Casoli, and D. Gogny, Microscopic approach of fission dynamics applied to fragment kinetic energy and mass distributions in ^{238}U , *Phys. Rev. C* **71**, 024316 (2005).
- [11] J.-F. Lemaître, S. Goriely, S. Hilaire, and J.-L. Sida, Fully microscopic scission-point model to predict fission fragment observables, *Phys. Rev. C* **99**, 034612 (2019).
- [12] K.-H. Schmidt, B. Jurado, C. Amouroux, and C. Schmitt, General description of fission observables: GEF model code, *Nucl. Data Sheets* **131**, 107 (2016), Special Issue on Nuclear Reaction Data.
- [13] P. Möller, D. G. Madland, A. J. Sierk, and A. Iwamoto, Nuclear fission modes and fragment mass asymmetries in a five-dimensional deformation space, *Nature (London)* **409**, 785 (2001).
- [14] P. Möller, J. Randrup, and A. J. Sierk, Calculated fission yields of neutron-deficient mercury isotopes, *Phys. Rev. C* **85**, 024306 (2012).
- [15] P. Möller and J. Randrup, Calculated fission-fragment yield systematics in the region $74 \leq Z \leq 94$ and $90 \leq N \leq 150$, *Phys. Rev. C* **91**, 044316 (2015).
- [16] D. Regnier, N. Dubray, N. Schunck, and M. Verrière, Fission fragment charge and mass distributions in $^{239}\text{Pu}(n, f)$ in the adiabatic nuclear energy density functional theory, *Phys. Rev. C* **93**, 054611 (2016).

- [17] H. Tao, J. Zhao, Z. P. Li, T. Nikšić, and D. Vretenar, Microscopic study of induced fission dynamics of ^{226}Th with covariant energy density functionals, *Phys. Rev. C* **96**, 024319 (2017).
- [18] D. Regnier, N. Dubray, and N. Schunck, From asymmetric to symmetric fission in the fermium isotopes within the time-dependent generator-coordinate-method formalism, *Phys. Rev. C* **99**, 024611 (2019).
- [19] J. Zhao, J. Xiang, Z.-P. Li, T. Nikšić, D. Vretenar, and S.-G. Zhou, Time-dependent generator-coordinate-method study of mass-asymmetric fission of actinides, *Phys. Rev. C* **99**, 054613 (2019).
- [20] C. Simenel, Particle Transfer Reactions with the Time-Dependent Hartree-Fock Theory Using a Particle Number Projection Technique, *Phys. Rev. Lett.* **105**, 192701 (2010).
- [21] G. Scamps, C. Simenel, and D. Lacroix, Superfluid dynamics of ^{258}Fm fission, *Phys. Rev. C* **92**, 011602(R) (2015).
- [22] M. Verriere, N. Schunck, and T. Kawano, Number of particles in fission fragments, *Phys. Rev. C* **100**, 024612 (2019).
- [23] M. Verriere and M. R. Mumpower, Improvements to the macroscopic-microscopic approach of nuclear fission, *Phys. Rev. C* **103**, 034617 (2021).
- [24] J. F. Berger, M. Girod, and D. Gogny, Microscopic analysis of collective dynamics in low energy fission, *Nucl. Phys. A* **428**, 23 (1984).
- [25] J. F. Berger, Quantum dynamics of wavepackets on two-dimensional potential energy surfaces governing nuclear fission, in *Dynamics of Wave Packets in Molecular and Nuclear Physics*, Lecture Notes in Physics Vol. 256, edited by J. Broeckhove, L. Lathouwers, and P. van Leuven (Springer, Berlin, 1986) p. 21.
- [26] W. Younes, D. M. Gogny, and J.-F. Berger, *A Microscopic Theory of Fission Dynamics Based on the Generator Coordinate Method*, Lecture Notes in Physics Vol. 950 (Springer International, Cham, 2019).
- [27] M. Verriere and D. Regnier, The time-dependent generator coordinate method in nuclear physics, *Front. Phys.* **8**, 233 (2020).
- [28] M. Warda, J. L. Egido, L. M. Robledo, and K. Pomorski, Self-consistent calculations of fission barriers in the Fm region, *Phys. Rev. C* **66**, 014310 (2002).
- [29] J. Zhao, T. Nikšić, D. Vretenar, and S.-G. Zhou, Microscopic self-consistent description of induced fission dynamics: Finite-temperature effects, *Phys. Rev. C* **99**, 014618 (2019).
- [30] H.-J. Mang, The self-consistent single-particle model in nuclear physics, *Phys. Rep.* **18**, 325 (1975).
- [31] J.-P. Blaizot and G. Ripka, *Quantum Theory of Finite Systems* (MIT Press, Cambridge, 1985).
- [32] M. Bender, P.-H. Heenen, and P.-G. Reinhard, Self-consistent mean-field models for nuclear structure, *Rev. Mod. Phys.* **75**, 121 (2003).
- [33] P. Ring and P. Schuck, *The Nuclear Many-Body Problem*, Texts and Monographs in Physics (Springer, Berlin, 2004).
- [34] N. Schunck, *Energy Density Functional Methods for Atomic Nuclei*, IOP Expanding Physics (IOP, Bristol, UK, 2019).
- [35] V. N. Fomenko, Projection in the occupation-number space and the canonical transformation, *J. Phys. A: Gen. Phys.* **3**, 8 (1970).
- [36] N. Schunck, D. Duke, H. Carr, and A. Knoll, Description of induced nuclear fission with Skyrme energy functionals: Static potential energy surfaces and fission fragment properties, *Phys. Rev. C* **90**, 054305 (2014).
- [37] N. Schunck, Z. Matheson, and D. Regnier, Microscopic calculation of fission fragment mass distributions at increasing excitation energies, in *Proceedings of the 6th International Workshop on Compound-Nuclear Reactions and Related Topics CNR*18*, Springer Proceedings in Physics, edited by J. Escher, Y. Alhassid, L. A. Bernstein, D. Brown, C. Fröhlich, P. Talou, and W. Younes (Springer, Berlin, 2020).
- [38] W. Reisdorf, J. P. Unik, H. C. Griffin, and L. E. Glendenin, Fission fragment K X-ray emission and nuclear charge distribution for thermal neutron fission of ^{233}U , ^{235}U , ^{239}Pu and spontaneous fission of ^{252}Cf , *Nucl. Phys. A* **177**, 337 (1971).
- [39] W. Lang, H.-G. Clerc, H. Wohlfarth, H. Schrader, and K.-H. Schmidt, Nuclear charge and mass yields for $^{235}\text{U}(n_{\text{th}}, f)$ as a function of the kinetic energy of the fission products, *Nucl. Phys. A* **345**, 34 (1980).
- [40] B. Ehrenberg and S. Amiel, Independent yields of krypton and xenon isotopes in thermal-neutron fission of ^{235}U . Observation of an odd-even effect in the element yield distribution, *Phys. Rev. C* **6**, 618 (1972).
- [41] S. Amiel and H. Feldstein, Odd-even systematics in neutron fission yields of ^{233}U and ^{235}U , *Phys. Rev. C* **11**, 845 (1975).
- [42] G. Mariolopoulos, C. Hamelin, J. Blachot, J. P. Bocquet, R. Brissot, J. Crançon, H. Nifenecker, and C. Ristori, Charge distributions in low-energy nuclear fission and their relevance to fission dynamics, *Nucl. Phys. A* **361**, 213 (1981).
- [43] J. P. Bocquet and R. Brissot, Mass, energy and nuclear charge distribution of fission fragments, *Nucl. Phys. A* **502**, 213 (1989).
- [44] F. Gönnewein, On the notion of odd-even effects in the yields of fission fragments, *Nucl. Instrum. Methods in Phys. Res. A* **316**, 405 (1992).
- [45] K.-H. Schmidt, S. Steinhäuser, C. Böckstiegel, A. Grewe, A. Heinz, A. R. Junghans, J. Benlliure, H.-G. Clerc, M. de Jong, J. Müller, M. Pfützner, and B. Voss, Relativistic radioactive beams: A new access to nuclear-fission studies, *Nucl. Phys. A* **665**, 221 (2000).
- [46] D. Ramos, M. Caamano, F. Farget, C. Rodriguez-Tajes, L. Audouin, J. Benlliure, E. Casarejos, E. Clement, D. Cortina, O. Delaune, X. Derkx, A. Dijon, D. Dore, B. Fernandez-Dominguez, G. de France, A. Heinz, B. Jacquot, A. Navin, C. Paradela, M. Rejmund *et al.*, Isotopic fission-fragment distributions of ^{238}U , ^{239}Np , ^{240}Pu , ^{244}Cm , and ^{250}Cf produced through inelastic scattering, transfer, and fusion reactions in inverse kinematics, *Phys. Rev. C* **97**, 054612 (2018).
- [47] A. Chatillon, J. Taieb, H. Alvarez-Pol, L. Audouin, Y. Ayyad, G. Belier, J. Benlliure, G. Boutoux, M. Caamano, E. Casarejos, D. Cortina-Gil, A. Ebran, F. Farget, B. Fernandez-Dominguez, T. Gorbinet, L. Grente, A. Heinz, H. T. Johansson, B. Jurado, A. Kelic-Heil *et al.*, Experimental study of nuclear fission along the thorium isotopic chain: From asymmetric to symmetric fission, *Phys. Rev. C* **99**, 054628 (2019).
- [48] C. Wagemans, E. Allaert, A. Deruytter, R. Barthelemy, and P. Schillebeeckx, Comparison of the energy and mass characteristics of the $^{239}\text{Pu}(n_{\text{th}}, f)$ and the $^{240}\text{Pu}(sf)$ fragments, *Phys. Rev. C* **30**, 218 (1984).
- [49] P. Geltenbort, F. Gönnewein, and A. Oed, Precision measurements of mean kinetic energy release in thermal-neutron-induced fission of ^{233}U , ^{235}U and ^{239}Pu , *Radiat. Eff.* **93**, 57 (1986).
- [50] P. Schillebeeckx, C. Wagemans, A. J. Deruytter, and R. Barthélémy, Comparative study of the fragments' mass and energy characteristics in the spontaneous fission of ^{238}Pu , ^{240}Pu

- and ^{242}Pu and in the thermal-neutron-induced fission of ^{239}Pu , *Nucl. Phys. A* **545**, 623 (1992).
- [51] K. Nishio, Y. Nakagome, I. Kanno, and I. Kimura, Measurement of fragment mass dependent kinetic energy and neutron multiplicity for thermal neutron induced fission of plutonium-239, *J. Nucl. Sci. Technol.* **32**, 404 (1995).
- [52] C. Tsuchiya, Y. Nakagome, H. Yamana, H. Moriyama, K. Nishio, I. Kanno, K. Shin, and I. Kimura, Simultaneous measurement of prompt neutrons and fission fragments for $^{239}\text{Pu}(n_{\text{th}},f)$, *J. Nucl. Sci. Technol.* **37**, 941 (2000).
- [53] R. Muller, A. A. Naqvi, F. Kappeler, and F. Dickmann, Fragment velocities, energies, and masses from fast neutron induced fission of ^{235}U , *Phys. Rev. C* **29**, 885 (1984).
- [54] G. Simon, J. Trochon, F. Brisard, and C. Signarbieux, Pulse height defect in an ionization chamber investigated by cold fission measurements, *Nucl. Instrum. Methods Phys. Res., Sect. A* **286**, 220 (1990).
- [55] S. Zeynalov, V. I. Furman, F. J. Hamsch, M. Florec, V. Y. Konovalov, V. A. Khryachkov, and Y. S. Zamyatnin, Investigation of mass-TKE distributions of fission fragments from the $^{235}\text{U}(n, f)$ -reaction in resonances, in *Proceedings of the 13th International Seminar on Interaction of Neutrons with Nuclei (ISINN-13) - Neutron Spectroscopy, Nuclear Structure, Related Topics* (Joint Institute for Nuclear Research, Dubna, Russia, 2006), Vol. 13, pp. 351–359.
- [56] C. Romano, Y. Danon, R. Block, J. Thompson, E. Blain, and E. Bond, Fission fragment mass and energy distributions as a function of incident neutron energy measured in a lead slowing-down spectrometer, *Phys. Rev. C* **81**, 014607 (2010).
- [57] A. Gook, F.-J. Hamsch, S. Oberstedt, and M. Vidali, Prompt neutrons in correlation with fission fragments from $^{235}\text{U}(n, f)$, *Phys. Rev. C* **98**, 044615 (2018).
- [58] W. Younes and D. Gogny, Nuclear Scission and Quantum Localization, *Phys. Rev. Lett.* **107**, 132501 (2011).
- [59] J. Sadhukhan, C. Zhang, W. Nazarewicz, and N. Schunck, Formation and distribution of fragments in the spontaneous fission of ^{240}Pu , *Phys. Rev. C* **96**, 061301(R) (2017).
- [60] B. Becker, P. Talou, T. Kawano, Y. Danon, and I. Stetcu, Monte Carlo Hauser-Feshbach predictions of prompt fission γ rays: Application to $n_{\text{th}} + ^{235}\text{U}$, $n_{\text{th}} + ^{239}\text{Pu}$, and ^{252}Cf (sf), *Phys. Rev. C* **87**, 014617 (2013).
- [61] A. J. M. Plompen, O. Cabellos, C. De Saint Jean, M. Fleming, A. Algora, M. Angelone, P. Archier, E. Bauge, O. Bersillon, A. Blokhin, F. Cantargi, A. Chebboubi, C. Diez, H. Duarte, E. Dupont, J. Dyrda, B. Erasmus, L. Fiorito, U. Fischer, D. Flammini *et al.*, The joint evaluated fission and fusion nuclear data library, JEFF-3.3, *Eur. Phys. J. A* **56**, 181 (2020).
- [62] A. C. Wahl, Systematics of fission-product yields, Los Alamos National Laboratory Technical Report No. LA-13928, 2002 (unpublished).
- [63] C. Schmitt, A. Guessous, J. P. Bocquet, H. G. Clerc, R. Brissot, D. Engelhardt, H. R. Faust, F. Gönnerwein, M. Mutterer, H. Nifenecker, J. Pannicke, C. Ristori, and J. P. Theobald, Fission yields at different fission-product kinetic energies for thermal-neutron-induced fission of ^{239}Pu , *Nucl. Phys. A* **430**, 21 (1984).
- [64] A. Bail, O. Serot, L. Mathieu, O. Litaize, T. Materna, U. Koster, H. Faust, A. Letourneau, and S. Panebianco, Isotopic yield measurement in the heavy mass region for ^{239}Pu thermal neutron induced fission, *Phys. Rev. C* **84**, 034605 (2011).
- [65] W. Nörenberg, Theory of mean primary charge distribution in low energy fission of even-even nuclei, *Z. Phys.* **197**, 246 (1966).
- [66] M. Caamano, F. Farget, O. Delaune, K. H. Schmidt, C. Schmitt, L. Audouin, C. O. Bacri, J. Benlliure, E. Casarejos, X. Derckx, B. Fernandez-Dominguez, L. Gaudefroy, C. Golabek, B. Jurado, A. Lemasson, D. Ramos, C. Rodriguez-Tajes, T. Roger, and A. Shrivastava, Characterization of the scission point from fission-fragment velocities, *Phys. Rev. C* **92**, 034606 (2015).
- [67] H. Naik, S. P. Dange, R. J. Singh, and S. B. Manohar, Systematics of charge distribution studies in low-energy fission of actinides, *Nucl. Phys. A* **612**, 143 (1997).
- [68] H. Naik, S. P. Dange, and A. V. R. Reddy, Charge distribution studies in the odd-Z fissioning systems, *Nucl. Phys. A* **781**, 1 (2007).
- [69] W. Younes and D. Gogny, Fragment yields calculated in a time-dependent microscopic theory of fission, Lawrence Livermore National Laboratory Technical Report No. LLNL-TR-586678, 2012 (unpublished).
- [70] A. Zdeb, A. Dobrowolski, and M. Warda, Fission dynamics of ^{252}Cf , *Phys. Rev. C* **95**, 054608 (2017).
- [71] P. Jaffke, P. Möller, P. Talou, and A. J. Sierk, Hauser-Feshbach fission fragment de-excitation with calculated macroscopic-microscopic mass yields, *Phys. Rev. C* **97**, 034608 (2018).
- [72] D. Lacroix and S. Ayik, Counting statistics in finite fermi systems: Illustrations with the atomic nucleus, *Phys. Rev. C* **101**, 014310 (2020).
- [73] K. T. R. Davies and J. R. Nix, Calculation of moments, potentials, and energies for an arbitrarily shaped diffuse-surface nuclear density distribution, *Phys. Rev. C* **14**, 1977 (1976).
- [74] N. Dubray and D. Regnier, Numerical search of discontinuities in self-consistent potential energy surfaces, *Comput. Phys. Commun.* **183**, 2035 (2012).
- [75] R. Bernard, H. Goutte, D. Gogny, and W. Younes, Microscopic and nonadiabatic Schrödinger equation derived from the generator coordinate method based on zero- and two-quasiparticle states, *Phys. Rev. C* **84**, 044308 (2011).
- [76] N. Schunck, D. Duke, and H. Carr, Description of induced nuclear fission with Skyrme energy functionals. II. Finite temperature effects, *Phys. Rev. C* **91**, 034327 (2015).
- [77] K. Dietrich, J.-J. Niez, and J.-F. Berger, Microscopic transport theory of nuclear processes, *Nucl. Phys. A* **832**, 249 (2010).